Energy Correlation among Three Photoelectrons Emitted in Core-Valence-Valence Triple Photoionization of Ne

Y. Hikosaka,[1] P. Lablanquie,[2,3] F. Penent,[2,3] J. Palaudoux,[2,3] L. Andric,[2,3] K. Soejima,[1] E. Shigemasa,[4] I. H. Suzuki,[5] M. Nakano,[5] and K. Ito[5]

[1]*Department of Environmental Science, Niigata University, Niigata 950-2181, Japan*
[2]*UPMC, Université Paris 06, LCPMR, 11 rue Pierre et Marie Curie, 75231 Paris Cedex 05, France*
[3]*CNRS, LCPMR (UMR 7614), 11 rue Pierre et Marie Curie, 75231 Paris Cedex 05, France*
[4]*UVSOR Facility, Institute for Molecular Science, Okazaki 444-8585, Japan*
[5]*Photon Factory, Institute of Materials Structure Science, Oho, Tsukuba 305-0801, Japan*

(Received 28 June 2011; published 9 September 2011)

The direct observation of triple photoionization involving one inner shell and two valence electrons is reported. The energy distribution of the three photoelectrons emitted from Ne is obtained using a very efficient multielectron coincidence method using the magnetic bottle electron spectroscopic technique. A predominance of the direct path to triple photoionization for the formation of Ne^{3+} in the $1s2s^22p^4$ configuration is observed. It is demonstrated that the energy distribution evolves with photon energy and indicates a significant difference with triple photoionization involving only valence electrons.

DOI: 10.1103/PhysRevLett.107.113005 PACS numbers: 32.80.Aa, 32.80.Fb, 32.80.Rm

In this Letter, we report the direct observation of core-valence-valence triple photoionization, together with the determination of energy sharing between three ejected photoelectrons.

Multiple photoionization processes through single photon absorption provide fundamental information both on electron correlations in the initial state and on the subsequent dynamics of the particles involved in the multiple ionization continuum. Double photoionization (DPI) of the helium atom, the prototype of three-body systems, can now be considered to be fully understood in view of the excellent agreement between the experimental measurements of the complete angular and energy correlations patterns, and the theoretical models [1,2]. Thus triple photoionization (TPI) is considered as the next frontier of the multiple photoionization study. The experimental study on TPI has, up to now, been largely limited to the measurement of the total cross sections [3,4]. Although complete energy and angular correlations between three electrons from TPI remain (and will remain) out of reach for experiment, it has been possible, for a state-of-the-art electron coincidence technique, to obtain energy correlation between the three electrons. However, valence TPI of rare gas atoms show, in practice, the prominence of sequential processes that mask the direct process with simultaneous emission of three electrons sharing the excess energy, and the visualization of the full figure of the energy correlation in the direct process is significantly interfered [5,6].

In this Letter we consider a new category of TPI process which involves a single core electron and two valence electrons. We have isolated the core-valence-valence TPI, with a very efficient multielectron coincidence method using the magnetic bottle electron spectroscopic technique [7]. A predominance of the direct TPI path is observed in Ne, and the full figure of the energy correlation is shown. The results presented in this Letter reveal that the direct process provides important information on multi-ionization mechanisms when, as in the present work, the electrons involved in the process initially originated from different shells.

The experiments were performed at the undulator beam line BL-16A of the Photon Factory. Single bunch operation of the storage ring provided a 624-ns repetition period for the 200-ps-width light pulses. Synchrotron radiation was monochromatized by a grazing incidence monochromator using a varied-line-spacing plane grating. A mechanical chopper in the form of a cylinder with 100 slots was employed to reduce the light repetition, and one light pulse every 12.5 μs was admitted into the interaction region [8]. Multicoincidences between electrons were recorded and analyzed in energy by their times of flight in a magnetic bottle electron spectrometer [7]. The description of the spectrometer and the data accumulation scheme is given elsewhere [8]. Conversion of the electron time of flight to kinetic energy was achieved by measuring the Ar photoelectron spectral lines at different photon energies. It was estimated that the energy resolving power of the apparatus $E/\Delta E$ was nearly constant at 60 for electrons of $E > 3$ eV, though ΔE was limited to around 20 meV (FWHM) for $E < 1$ eV. The measured detection efficiency decreases slowly with electron kinetic energy from $75 \pm 5\%$ ($E = 0$ eV) to $43 \pm 5\%$ ($E = 800$ eV). Multielectron coincidence data sets were accumulated for Ne at three different photon energies ($h\nu = 1050$, 1150, and 1250 ± 0.5 eV), where the photon bandwidths were set to around 2 eV.

First, we describe the procedure to understand how to extract information from multicoincidence events in the accumulated coincidence data, to isolate the particular

TPI from other (dominant) photoionization processes. Figure 1(a) shows a histogram of the sum of the energies of two electrons, derived from the data accumulated at $h\nu = 1150$ eV, which is plotted also as a function of binding energy of Ne^{2+}. The energy range covers the structures for the Ne^{2+} states formed by core-valence DPI [9]. Here, only the multielectron coincidence events involving a fast electron in the kinetic energy region of 650–900 eV are accepted in the analysis, as it is expected that only core-valence ionized Ne^{2+} states emit Auger electrons enough in such kinetic energy region. This restriction considerably reduces the background contribution. For the sake of simplicity, the kinetic energy of electron i is denoted by E_i with $i = 1, 2, \ldots, n$. The index $i = 1$ corresponds to the fastest electron and $i = n$ to the slowest. With this notation, the curve in Fig. 1(a) is defined as a plot of $E_2 + E_3$ for the events in the condition of $E_1 = 650$–900 eV.

Figure 1(a) exhibits the formation of the Ne^{2+} $1s^{-1}2p^{-1}$ and $1s^{-1}2s^{-1}$ states [9]. In addition, complex structures assignable to satellite states with configurations of $1s^{-1}2p^{-2}nl$ are identified in the binding energy range of 965–990 eV. Since these satellite Ne^{2+} states have

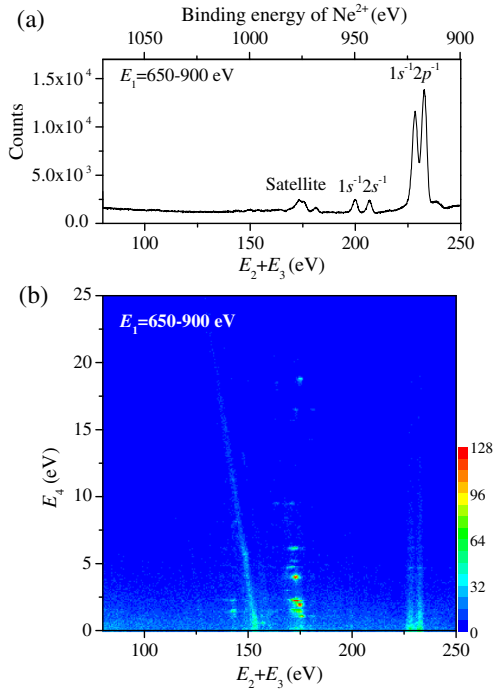

FIG. 1 (color online). (a) Histogram of the sum of the energies of two electrons emitted at $h\nu = 1150$ eV in Ne, displaying the Ne^{2+} states populated via core-valence DPI. (b) Two-dimensional map showing the coincidences of three electrons, plotted as a function of sum of the two electrons energies [common to the horizontal axis in (a)] and of the third slow electron. Only multielectron coincidence events including a fast electron in the kinetic energy range of 650–900 eV are used in the analysis.

Rydberg state character with a Ne^{3+} $1s^{-1}2p^{-2}$ core associated to core-valence-valence TPI, the corresponding Ne^{3+} states should lie at higher binding energies than these Ne^{2+} satellite states. However, as the available energy in the Ne^{3+} formation is shared among three photoelectrons, no tangible structure associated with the Ne^{3+} formation is discernible in this plot of $E_2 + E_3$.

Figure 1(b) displays the energy correlation map showing the coincidences of three electrons, where the horizontal axis corresponds to $E_2 + E_3$, in common with the horizontal axis of Fig. 1(a), and the vertical one does to the energy of another slower electron, E_4. Here, similarly, only the coincidence events including a fast electron in $E_1 = 650$–900 eV are adopted. On this energy correlation map, a diagonal stripe is clearly observed in the region of $E_2 + E_3 < 160$ eV. This stripe traces a line of $E_2 + E_3 + E_4 =$ const, which agrees with the condition required for a core-valence-valence TPI structure. Apart from such diagonal stripe, other structures are observed on the map: Two vertical stripes seen at $E_2 + E_3$ corresponding to the formation of the Ne^{2+} $1s^{-1}2p^{-1}$ states are produced through the direct double Auger decay from these Ne^{2+} states, and knots of enhancements at given E_4, observed in the $E_2 + E_3$ range corresponding to the formation of the Ne^{2+} satellite states, are due to the cascade double Auger decay from the Ne^{2+} satellite states.

To locate the Ne^{3+} states formed by core-valence-valence TPI, the coincidence counts on the map in Fig. 1(b) are projected onto an axis defined by $E_2 + E_3 + E_4$. Figure 2(a) shows the projection curve (black or solid) as a function of $E_2 + E_3 + E_4$, and also of binding energy of Ne^{3+}. When the projection is restricted to the events with $E_4 > 5$ eV, the background contribution in the projection curve (red or dotted) is largely reduced. The effective reduction of the background contribution is due to the large false coincidence counts in the low E_4 range in Fig. 1(b). One can find in the projection curves a large peak at the binding energy of 995 eV, which corresponds to the diagonal stripe clearly seen in Fig. 1(b). In addition, the high statistics arising from the projection enables us to find other weak peaks.

The spectroscopic symmetries of the observed peaks can be deduced from a comparison with the MCSCF calculations of energy levels of the Ne^{3+} states [10]. The accuracy of the theoretical results, although subject to an overall error of around 3 eV, is sufficient to make a reliable assignment of the peaks observed in Fig. 2(a). Here, the relative peak intensities do not reflect the statistical values of these assigned states. In particular, a significant formation of the ^2D and/or ^2P component(s) of Ne^{3+} $1s^{-1}2p^{-2}$ is observed. Such nonstatistical populations of formed ion levels are widely observed in DPI [7,11] and TPI [5].

The two-dimensional map in Fig. 2(b) shows the E_1 distributions at each $E_2 + E_3 + E_4$. Thus, the vertical structures at $E_2 + E_3 + E_4$ of each Ne^{3+} state delineate

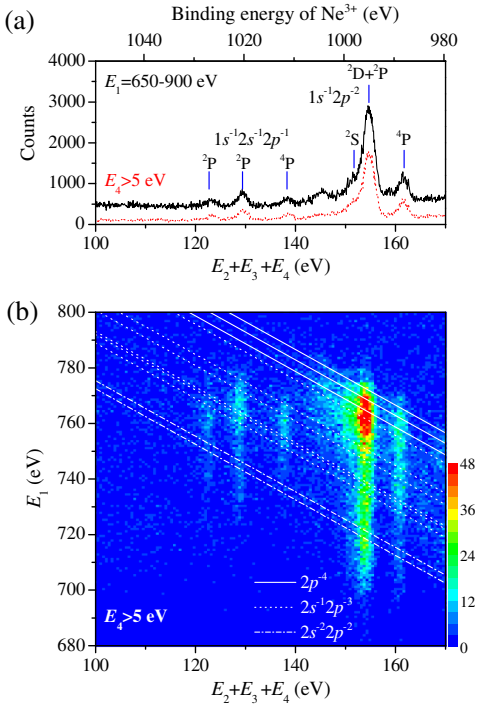

FIG. 2 (color online). (a) Distributions of the kinetic energy sum for the three slowest electrons detected as fourfold coincidences; they correspond to projections of the counts in Fig. 1(b) onto an axis of $E_2 + E_3 + E_4$. While the black or solid curve results from the projection for the whole area in Fig. 1(b), the red or dotted one from the projection for a limited area of $E_4 > 5$ eV. (b) Two-dimensional map showing Auger electron distributions in coincidences with the structures displayed in (a), where only the events of $E_4 > 5$ eV are adopted.

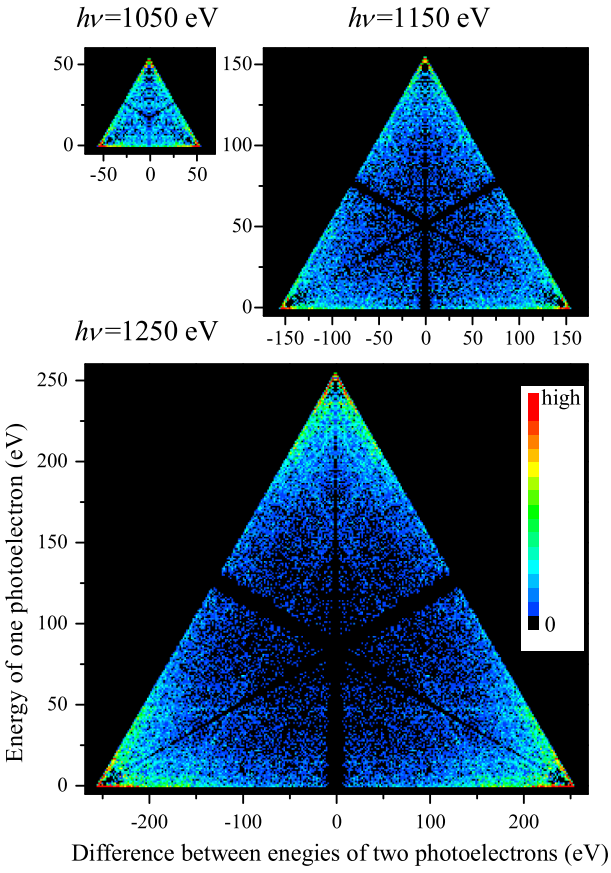

FIG. 3 (color online). Dalitz plot representation of the energy correlations among the three photoelectrons emitted in core-valence-valence TPI for the formation of Ne^{3+} $1s^{-1}2p^{-2}$ ($^2S + {}^2D$). In these plots, only four-electron coincidence events including a fast Auger electron in a narrow E_1 range of 750–775 eV were adopted. Since the important Auger intensity is concentrated in this E_1 range [see Fig. 2(b)], this restriction reduces background contributions from false coincidences. The background contributions due to false coincidences, estimated from the same extractions for different E_1 ranges, were subtracted. The gaps seen as asterisklike shapes on the maps are due to the detection dead time arising from inseparable electron signals.

the distributions of Auger electrons. Although the formation of individual Ne^{4+} levels is not resolved due to the limited energy resolution for such fast electrons, formation of individual Ne^{4+} levels necessarily falls on the diagonal lines indicated on the map. One can find that the Auger final Ne^{4+} levels are dependent on the initial Ne^{3+} states: While Auger decay from the Ne^{3+} $1s^{-1}2p^{-2}$ states largely populates Ne^{4+} $2p^{-4}$, the Ne^{3+} $1s^{-1}2s^{-1}2p^{-1}$ states favorably decay into Ne^{4+} $2s^{-1}2p^{-3}$. Thus, during the Auger decay of the $1s$ core hole the involvement of the $2s$ inner shell is weak.

Based on the ability to isolate core-valence-valence TPI, we illustrate how the energy distributions of the three photoelectrons reflect the TPI dynamics. Figure 3 represents the energy distributions for the Ne^{3+} $1s^{-1}2p^{-2}$ ($^2D + {}^2P$) formation, extracted from three sets of different photon energy data. Introducing a variant of the Dalitz plot [12] to visualize the energy distribution of the three photoelectrons [13], coincidence yields are plotted as a function of the energy difference of two photoelectrons and of the energy of the third photoelectron. The resulting two-dimensional map yields complete information on the energy distributions of the three electrons. Here, the energies of the three electrons are given by the distance to the three sides of the triangle.

On these maps, sequential TPI processes would yield island or line structures, because in such processes at least one of the Auger electrons has to have a fixed energy. Indeed, line structures running parallel to the sides of the triangles are weakly discernible on the maps, where the notable ones are ascribable to DPI into Ne^{2+} $1s^{-1}2s^{-2}nl$ and the autoionization; however, the contribution from such sequential TPI processes seems to be only a minor path in the total Ne^{3+} $1s^{-1}2p^{-2}$ ($^2D + {}^2P$) formation and that simultaneous emission of the three photoelectrons is the dominant path accordingly. This observation is in striking contrast to the valence TPI in Ne [6] and in Ar [5] where predominant contributions from sequential

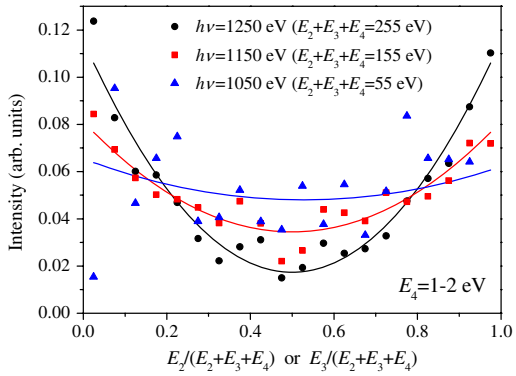

FIG. 4 (color online). Kinetic energy distributions of the two photoelectrons emitted together with a slow photoelectron of $E_4 = 1$–2 eV in TPI into Ne^{3+} $1s2s^22p^4$ $(^2S + {}^2D)$, at $h\nu =$ 1050, 1150, and 1250 eV. The contributions from false coincidences were subtracted. The solid curves are fittings assuming a parabola function.

TPI via intermediate doubly charged levels are observed. One can find in Fig. 3 that, at the lowest photon energy, the counts tend to be spread over the whole area, and, as photon energy increases, the intensity at the corner areas of the triangle gradually increases. In other words, with increasing available energy, the three photoelectrons preferably have unequal energy sharings in which one electron has a large energy and both other two electrons have low energies. The present work has succeeded in demonstrating such a pattern of energy sharing experimentally, confirming the theoretical prediction [14,15].

The unequal energy sharing observed at high energy may be interpreted in terms of double shakeoff: the sudden change in central potential upon ejection of a core electron leads to the additional emission of two slow electrons from valence orbitals. In this case, the fastest electron originates from the $1s$ shell and the other two slow electrons from the $2p$ shell. On the other hand, from the knowledge concerning DPI, one supposes an important contribution from knockout process at low available energy. The rather flat distribution seen at $h\nu = 1050$ eV may suggest the contribution from a double knockout process in which the primary-outgoing $1s$ electron knocks out two valence electrons, by analogy with the flat energy distributions seen in DPI due to the knockout process.

Figure 4 plots the energy distributions of the two faster photoelectrons emitted in formation of Ne^{3+} $1s^{-1}2p^{-2}$ $(^2D + {}^2P)$, for events selected by restricting the slowest photoelectron energy to $E_4 = 1$–2 eV. This choice of E_4 is for comparison with the energy distribution reported for the valence TPI in Ar [5]. The distributions in Fig. 4 show U-shape profiles, which become deeper with increasing photon energy, as seen in Fig. 3. However, compared with valence TPI in Ar at an available energy of 148 eV [5], the shape is less deep even at an available energy of 255 eV. The shallowing of the distribution in the core-valence-valence TPI in Ne may suggest a more important knockout contribution included in this TPI. On the other hand, even the shakeoff picture can interpret the observation: Since the central potential, to which the valence electrons are subject, should change more drastically on the ejection of a core electron than on that of another valence electron, the energy distribution of the shaken-off valence electrons would extend to higher energy.

It is likely that either reasoning results in a more favorable intensity in the core-valence-valence TPI case than in the valence TPI. The total intensity for core-valence-valence TPI, compared to the intensity of the core single photoionization, is estimated, from the coincidence counts and the detection efficiency, to be around 2%–5% at the measured three photon energies. While ~1.4% intensity compared to the single photoionization is reported in valence TPI of Ne at available energy range of 150–350 eV [16], the intensity mainly results from sequential paths [6]. This fact suggests that the direct path in the core-valence-valence TPI is more favorable, in relative intensity compared to the relevant single photoionization, than that in the valence TPI.

In conclusion, we have directly observed core-valence-valence TPI. Energy distributions of the three emitted photoelectrons leading to the formation of Ne^{3+} $1s^{-1}2p^{-2}$ $(^2D + {}^2P)$ reveals a predominant contribution from the direct path, in striking contrast to the observations in valence TPI [5,6]. The energy correlations among the three photoelectrons visualize the evolution of the four-body Coulomb dynamics with photon energy. The double differential cross sections derived from the energy correlations show U-shape profiles, which are less deep than that observed in the valence TPI of Ar. This observation suggests more effective double knockout and/or double shakeoff on ejection of a core electron than on ejection of a same-orbital valence electron. A theoretical interpretation of the process would be desirable in order to more fully understand the TPI dynamics.

We warmly thank Ronald McCarroll for useful discussions and a critical reading of the manuscript. We are grateful to the Photon Factory staff for the stable operation of the PF ring. Financial support from JSPS and CNRS are acknowledged. This work was performed with the approval of the Photon Factory Program Advisory Committee (proposals No. 2008G529 and No. 2010G621).

[1] J. S. Briggs and V. Schmidt, J. Phys. B **33**, R1 (2000).
[2] L. Avaldi and A. Huetz, J. Phys. B **38**, S861 (2005).
[3] R. Wehlitz *et al.*, Phys. Rev. Lett. **81**, 1813 (1998).
[4] R. Wehlitz *et al.*, Phys. Rev. A **61**, 030704(R) (2000).
[5] Y. Hikosaka *et al.*, Phys. Rev. Lett. **102**, 013002 (2009).
[6] L. Andric *et al.* (unpublished).
[7] J. H. D. Eland *et al.*, Phys. Rev. Lett. **90**, 053003 (2003).
[8] K. Ito *et al.*, Rev. Sci. Instrum. **80**, 123101 (2009).
[9] Y. Hikosaka *et al.*, Phys. Rev. Lett. **97**, 053003 (2006).

[10] N. Mårtensson, S. Svensson, and U. Gelius, J. Phys. B **20**, 6243 (1987).
[11] K.-H. Schartner *et al.*, J. Phys. B **26**, L445 (1993).
[12] R. H. Dalitz, Philos. Mag. **44**, 1068 (1953).
[13] P. Lablanquie *et al.*, Phys. Chem. Chem. Phys. (to be published).
[14] J. Colgan and M. S. Pindzola, J. Phys. B **39**, 1879 (2006).
[15] A. Emmanouilidou and J. M. Rost, J. Phys. B **39**, L99 (2006).
[16] N. Saito and I. H. Suzuki, Phys. Scr. **49**, 80 (1994).